PAPER

Check for updates

A synthetic method for lanthanum hydroxychloride suitable for industrialization and its thermal decomposition properties†

Hao Tian, ‡[ab] Jincheng Guo, ‡*[b] Yu Pei,[b] Shaochun Hou,[b] Yuanjiang Wang[b] and Yumei Xia[b]

A reactive crystallization method for the synthesis of lanthanum hydroxychloride (La(OH)$_2$Cl) was developed to provide a new low-carbon route for the purification of rare earth elements in hydrometallurgy. The synthetic method reported herein represents a unique low-temperature route, short preparation time and inexpensive materials compared with previous methods, thus making it promising for industrial applications. The key factors controlling the product's phase were determined using single factor tests involving temperature, concentration of NH$_4$Cl in the base solution and the molar ratio of NH$_4$OH/La^{3+} added per minute into the base solution. Otherwise, the outcome is lanthanum hydroxide (La(OH)$_3$). Subsequently, the synthesized products were characterized by employing X-ray diffraction (XRD), Fourier transform infrared (FT-IR) spectroscopy, transmission electron microscopy (TEM), and energy dispersive spectroscopy (EDS). Finally, the thermal decomposition behavior of La(OH)$_2$Cl was assessed using thermogravimetry (TG) and differential scanning calorimetry (DSC). Lanthanum oxychloride (LaClO) was obtained at about 360 °C. The thermal transformation from LaClO to La$_2$O$_3$ started at 400 °C and was a slow oxidation process. Pure La$_2$O$_3$ could be obtained when the temperature increased to 1500 °C.

1. Introduction

Rare earth ions are extracted *via* ammonium bicarbonate precipitation in the rare earth hydrometallurgy process.[1,2] However, massive amounts of carbon dioxide are released in this mainstream technology.[3] Some carbon dioxide is produced during the reaction, and the rest arises from thermal decomposition to obtain rare earth oxide. However, weather patterns have become more volatile, and extremes have become more common as global warming continues.[4] Therefore, low-carbon development in all sectors is put forward to solve this problem.[5,6] Therefore, low-carbon reforms in the purification process of rare earth elements is imperative.

Lanthanide hydroxychloride (Ln(OH)$_2$Cl) has a monoclinic structure in which the adjacent layers are predominantly held by O–H···Cl hydrogen bonds.[7–9] It can be decomposed into lanthanum oxychloride through calcination, as per the

equation: Ln(OH)$_2$Cl → LnOCl + H$_2$O (↑).[7,10,11] Moreover, Ln(OH)$_2$Cl can be further decomposed into rare earth oxides in an air atmosphere at over 1050 °C.[12,13] Water and chlorine are the byproducts produced during this thermal decomposition process. In other words, thermal decomposition is advantageous over the current practice of preparing rare earth oxides from rare earth carbonates as it can significantly reduce carbon emissions. Moreover, no carbon dioxide is produced during Ln(OH)$_2$Cl precipitation. It presents a distinctive and transparent approach for advancing a low-carbon economy in the metallurgical processing of rare earth elements.

However, currently, there are limited methods available for the synthesis of Ln(OH)$_2$Cl. The hydrothermal method is the most commonly used (Table 1), but it requires specialized equipment to reach high temperatures and pressures, and it can be hardly applied to the industrial process. Thus, in this work, we developed a reactive crystallization method to synthesize lanthanum hydroxychloride without using any surfactant, chelating agent, gelating agent or extreme conditions. The operation is simple, convenient, and fit for industrialization. We selected lanthanum for the experiments because of its sufficient reserves and single valence and investigated the necessary factors for synthesizing La(OH)$_2$Cl. Finally, we explored the thermal decomposition properties of lanthanum hydroxychloride.

aInner Mongolia Key Laboratory of Ferroelectric-Related New Energy Materials and Devices, School of Materials and Metallurgy, Inner Mongolia University of Science and Technology, Baotou 014010, China

bState Key Laboratory of Baiyunobo Rare Earth Resource Researches and Comprehensive Utilization, Baotou Research Institute of Rare Earth, Baotou 014030, China. E-mail: 2120160813@mail.nankai.edu.cn

‡ H. Tian and J. C. Guo contributed to the work equally and should be regarded as cofirst authors.

Table 1 The contrast between previously reported methods and our method for the synthesis of La(OH)$_2$Cl

Quote	Method	Temperature	Time	Materials
Carter et al., 1969 (ref. 8)	Hydrothermal method	500 °C	2–5 days	NH$_4$Cl, AlCl$_3$·6H$_2$O, HNO$_3$, HCl
Jouve et al., 2002 (ref. 14)	Hydrothermal method	200 °C	2 days	Sm$_2$O$_3$, NH$_4$Cl
Mahajan et al., 2008 (ref. 15)	Thermally assisted hydrolysis	130 °C	32 h	EuCl$_3$·6H$_2$O, [CH$_3$(CH$_2$)$_7$]$_3$PO, NaOH
Lee et al., 2008 (ref. 7)	Solvothermal method	600 °C	10 h	LaCl$_3$·7H$_2$O, TmCl$_3$, ethanol
Kim et al., 2017 (ref. 16) and Soto-Donoso et al., 2023 (ref. 17)	Liquid preparation method	90 °C	12 h	LaCl$_3$, NaCl, ethylenediamine
Dunn et al., 2020 (ref. 18)	Solvothermal method	240 °C	24 h	LnCl$_3$·7H$_2$O, polyethylene glycol
Fellner et al., 2021 (ref. 19)	Microwave solvothermal method	150/200 °C	≤1 h	LuCl$_3$, benzyl alcohol, Eu(Ac)$_3$
This work	Homogeneous preparation method	60–80 °C	4 h	LaCl$_3$, NH$_4$OH, NH$_4$Cl, water

Table 2 Chemical compositions of an aqueous solution of lanthanum chloride (g L^{-1})

Elements	REO	MgO	Al$_2$O$_3$	Na$_2$O	CaO	ZnO	Fe$_2$O$_3$
Concentration	303.7	0.023	0.022	<0.005	0.039	0.680	<0.005

2. Experiment

2.1 Materials and chemical analysis methods

An aqueous solution of lanthanum chloride was offered by China Northern Rare Earth (Group) High-Tech Co., Ltd, and its chemical composition is listed in Table 2. The total rare earth content was measured using the EDTA (ethylene diamine tetraacetic acid) complexometric titration method, while the ion impurities were measured by the ICP (Inductively Coupled Plasma) method. Other chemical agents used in our experiments were of analytical grade and used as received without further purification.

2.2 Preparation procedure

In this experiment, a parallel flow feeding mode was utilized to decrease the supersaturation of this reaction system (Fig. 1). It is helpful to form large and uniform crystal size. To achieve the desired concentration (100 g L^{-1}) of lanthanum chloride solution, a 66 mL rare earth solution was diluted with 154 mL of distilled water. The reason why we used rare earth chloride is because it is the extraction product in the rare earth hydrometallurgy process. The precipitant was prepared by diluting 45 mL of commercial ammonia (13.38 M) with 105 mL of distilled water. Subsequently, these solutions were simultaneously added dropwise to ammonium chloride aqueous
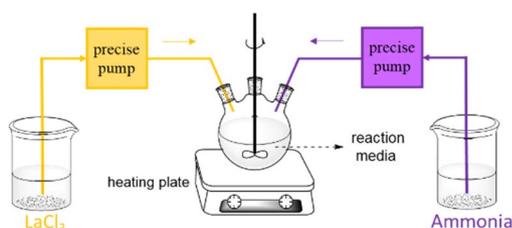

Fig. 1 Schematic of the reaction setup.

solutions with varying concentrations and temperatures. Ammonium chloride aqueous can provide an abundance of chloride ions. Also, a certain temperature can not only offer the energy of product formation but also decrease the supersaturation. Notably, we investigated the effect of the molar ratio of NH$_4$OH/La^{3+} dropped per minute into the base solution by adjusting the feeding rate of ammonia. We found three major factors, namely, temperature, concentration of NH$_4$Cl in the base solution and the molar ratio of NH$_4$OH/La^{3+} dropped per minute into the base solution, through a great number of experiments. In this paper, they were examined and are summarized in Table 3. The resulting products were promptly collected under the aforementioned conditions using a Buchner funnel, washed three times with distilled water, and dried in an oven at 70 °C. Parallel experiments were performed to ensure the accuracy of the experimental result.

2.3 Instrumentation

Powder X-ray diffraction (XRD) patterns were collected on a DX-27 mini X-ray diffractometer (Dandong Haoyuan Instrument Co., Ltd, China) using Cu Kα radiation with a step size of 0.02° from 5 to 90°. Fourier transform infrared (FT-IR) spectra were recorded using KBr pellets on a Nicolet iS 10 spectrophotometer (Thermo Fisher Scientific Inc., USA). Transmission electron microscopy (TEM) images and high-resolution TEM (HRTEM) images were obtained on a Talos F200i transmission electron microscope (Thermo Fisher Scientific Inc., USA) with an accelerating voltage of 200 kV. Thermogravimetry-differential scanning calorimetry (TG-DSC) analyses were carried out using an STA449 F3 simultaneous thermal analyzer (NETZSCH, Germany) in an air atmosphere in the temperature range from room temperature to 800 °C, and the heating rate was 5 °C min^{-1}. Field emission-scanning electron microscopy (FE-SEM) images were collected on a Sigma 500 electron microscope electron microscope (Carl Zeiss, Germany) operating at 15 kV.

3. Results and discussion

3.1 Effect of the key factors on the phase of the product

Fig. 2 compares the wide-angle XRD patterns of samples 1 and 5, which were selected as representatives due to their extreme

Table 3 Major experimental conditions for the preparation

Sample no.	Temperature (°C)	Concentration of NH$_4$Cl (M)	Feeding rate of ammonia (mL min^{-1})	Molar ratio of NH$_4$OH/La^{3+} dropped per minute
1	80	1.0	0.38	3.0
2	80	1.8	0.38	3.0
3	80	2.0	0.38	3.0
4	80	3.0	0.38	3.0
5	80	4.0	0.38	3.0
6	70	1.0	0.38	3.0
7	70	2.0	0.38	3.0
8	70	2.8	0.38	3.0
9	70	3.0	0.38	3.0
10	70	4.0	0.38	3.0
11	60	3.0	0.38	3.0
12	60	4.0	0.38	3.0
13	80	2.0	0.37	2.9
14	80	2.0	0.39	3.1
15	80	4.0	0.39	3.1
16	80	1.0	0.21	2.0
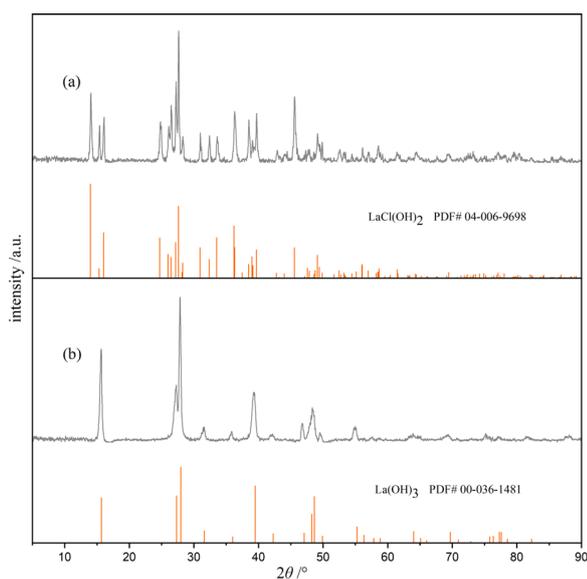
Fig. 2 XRD patterns of (a) sample 5 and (b) sample 1.

synthesis conditions. The others are shown in the ESI.† As shown in Fig. 2a, the diffraction peaks centered at $2\theta = 13.96°$, 16.02°, 24.69°, 27.59°, 27.19°, 33.52°, 36.21°, and 36.30° correspond to the reflection planes of (001), (−101), (101), (−111), (110), (111), (012), and (−211), respectively, for La(OH)$_2$Cl. These peaks are consistent with the monoclinic phase structure of La(OH)$_2$Cl, with the space group of $P2_1/m$. Also, no additional diffraction peaks of other impurity phases are observed. Besides, the positions and relative intensities of the diffraction peaks in Fig. 2b are indexed to the hexagonal structure of La(OH)$_3$ with a space group of $P6_3/m$.

Table 4 displays the phase of the product formed, determined from the XRD patterns of samples 1–16 (detailed XRD patterns for each sample are provided in the ESI,† as shown in Fig. S2 to S17†). The results indicate that the product obtained

at 80 °C is La(OH)$_2$Cl if the concentration of NH$_4$Cl in the base solution is equal to or greater than 2 mol L^{-1}. On the other hand, if the concentration of NH$_4$Cl is less than 2 mol L^{-1}, the resulting product is La(OH)$_3$ instead of La(OH)$_2$Cl. This result shows that the concentration of chloride ion is significant for the production of La(OH)$_2$Cl. At a lower reaction temperature of 70 °C, the concentration of NH$_4$Cl must increase to 3 mol L^{-1} to obtain La(OH)$_2$Cl. However, at a reaction temperature of 60 °C, La(OH)$_2$Cl precipitation cannot be obtained under any conditions. This indicates that the formation of La(OH)$_2$Cl needs enough energy to go over the barrier. It is important to note that the above conclusions are valid only if the molar ratio of NH$_4$OH/La^{3+} dropped per minute into the base solution is less than or equal to 3. From the results of samples 14 and 15, it is inferred that when the molar ratio of NH$_4$OH/La^{3+} exceeds 3, the resulting product is La(OH)$_3$. This outcome suggests that it is not conducive to form La(OH)$_2$Cl when the reaction system is too alkaline. Additionally, the results of sample 16 reveal that if the concentration of NH$_4$Cl does not meet the required standards, we cannot obtain the desired product. Again, the concentration of chloride ion is a crucial effect factor. To sum up, the production of La(OH)$_2$Cl needs sufficient energy, sufficient concentration of chloride ion and lower alkaline reaction system. Also, it is necessary to control the several experimental parameters simultaneously to meet the formation conditions.

Table 4 Experimental phase of the product formed and yield

Sample no.	Phase	Yield	Sample no.	Phase	Yield
1	La(OH)$_3$	—	9	La(OH)$_2$Cl	97.14%
2	La(OH)$_3$	—	10	La(OH)$_2$Cl	96.34%
3	La(OH)$_2$Cl	97.55%	11	La(OH)$_3$	—
4	La(OH)$_2$Cl	97.10%	12	La(OH)$_3$	—
5	La(OH)$_2$Cl	99.16%	13	La(OH)$_2$Cl	96.73%
6	La(OH)$_3$	—	14	La(OH)$_3$	—
7	La(OH)$_3$	—	15	La(OH)$_3$	—
8	La(OH)$_3$	—	16	La(OH)$_3$	—

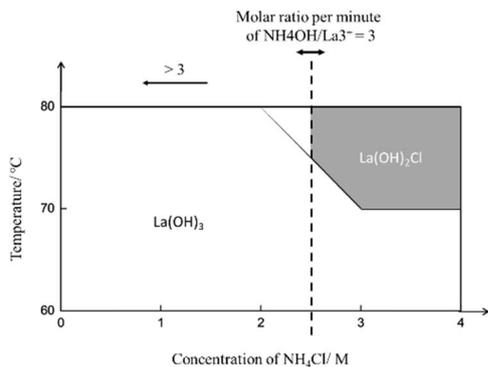**Fig. 3** Schematic of the cooperative effect of the molar ratio of NH_4OH/La^{3+} added per minute, temperature, and concentration of NH_4Cl on the phase of the product.

Fig. 3 presents a schematic illustration that aims to explain the cooperative effect of the three experimental factors mentioned above on the phase of the product. The gray area, including the borderline, represents the only region where the $La(OH)_2Cl$ product is obtained. The dashed line in this illustration implies that the molar ratio of NH_4OH/La^{3+} dropped per minute in the base solution is equal to 3 and can move left and right. The area to the left of the dashed line indicates that the molar ratio is greater than 3. Furthermore, as the line moves from the left to the right, the region to the left of the dashed line turns white, implying the formation of $La(OH)_3$.

3.2 Morphologies of $La(OH)_2Cl$

The surface morphologies and crystal structures of the as-prepared $La(OH)_2Cl$ were depicted through the TEM images. The TEM images of samples 3–5 are presented in Fig. 4a–c. Noticeably, at an NH_4Cl aqueous solution concentration of 2 mol L^{-1}, the morphology of the product consists of rectangular-column and rod-shaped particles. This outcome suggests that the crystallinity is low, and the rod-shaped particles separate from the rectangular-column-shaped particles due to a partial hydrogen bond fracture between the layers.
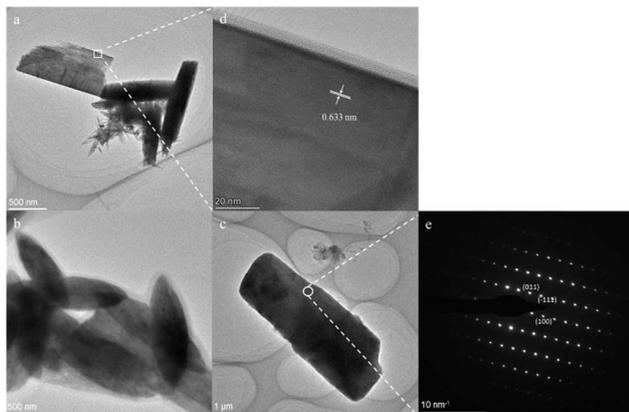
However, the monocrystals have spindle and more complete rectangular-column shapes at concentrations of 3 mol L^{-1} and 4 mol L^{-1}. Beside, these results also reveal the possible assembly process of the bulk crystalline $La(OH)_2Cl$ during this synthesis method. The structural effects of $La(OH)_2Cl$ result in the 0D structures undergoing oriented attachment, producing a single elongated structure in the initial stage. During the process of crystal growth, the rod-shaped crystals aggregate into bundles, which gradually evolve into spindle-shaped and then rectangular-column-shaped crystals, mirroring the evolution observed during the synthesis of nanostructured $Eu(OH)_2Cl$ from Eu_2O_3 nanocrystals. Hence, based on the above conclusion, the optimal experimental conditions are as follows: a temperature of 80 °C, a base solution with an NH_4Cl concentration of 4 mol L^{-1}, and a molar ratio of NH_4OH/La^{3+} dropped per minute of 3. Moreover, Fig. 5d displays the lattice spacings from the HRTEM image of the local area marked by the white box in Fig. 4a, revealing the highly crystalline quality of $La(OH)_2Cl$. The measured interplanar distance is approximately 0.633 nm, corresponding to the (100) plane of monoclinic $La(OH)_2Cl$. Further, Fig. 4e depicts the selected area electron diffraction (SAED) pattern obtained from the sample in Fig. 5c, indexed to the monoclinic phase of $La(OH)_2Cl$, as confirmed by the XRD data.

3.3 Composition of $La(OH)_2Cl$

Fig. 5 illustrates the use of FTIR spectroscopy for examining the chemical bonding on the surface of the as-synthesized $La(OH)_2Cl$ (sample 5). The sharp peaks observed at 3565 cm^{-1} and 3610 cm^{-1} are associated with the vibration of O–H bonds in $La(OH)_2Cl$,[20] while the broad absorption at about 3500 cm^{-1} is ascribed to the stretching vibration of water.[12] The spectrum displays two absorption peaks of O–H bonds resulting from OH···Cl hydrogen bonds. The weak peaks at 1390 cm^{-1}, 1496 cm^{-1}, and 1628 cm^{-1} correspond to the carbonate species absorbed from the atmosphere.[21] Moreover, the band at 674 cm^{-1} is identified as the stretching vibration of La–O bonds.[22,23] Finally, the strong peaks at 419 cm^{-1} and 567 cm^{-1} are attributed to the stretching vibration and normal vibrational mode of the La–O bond, respectively.[21,24] These results provide strong evidence for the formation of $La(OH)_2Cl$, which is in accordance with the XRD results (Fig. 2a).
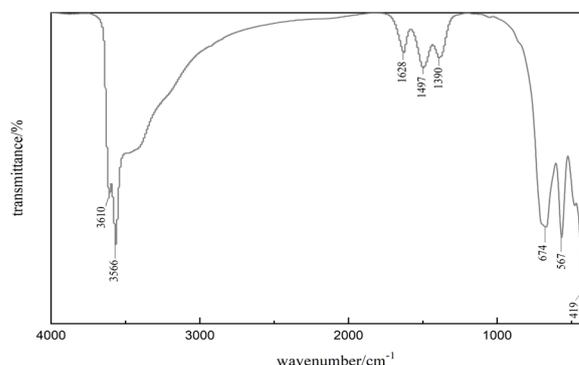

Fig. 4 TEM images of sample 3 (a), sample 4 (b), and sample 5 (c). (d) The HRTEM image of the selected area in figure. (a). (e) SAED pattern of the selected area marked in (c).

Fig. 5 FT-IR spectra of the as-synthesized $La(OH)_2Cl$ (sample 5).

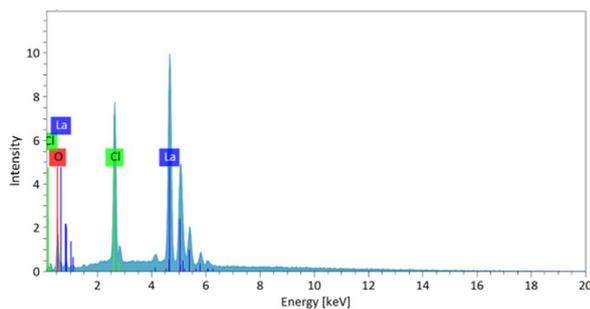**Fig. 6** EDS patterns of as-synthesized La(OH)$_2$Cl (sample 5).

Energy dispersive spectroscopy (EDS) analysis was employed to determine the composition of the as-synthesized La(OH)$_2$Cl (sample 5). As shown in Fig. 6, EDS clearly identified that the crystalline substances are composed of Cl, O and La and should therefore be attributed to La(OH)$_2$Cl; H cannot be detected by EDS, thus further confirming the purity of the products. This result is in agreement with the XRD data.

3.4 Thermal analysis

Next, the TG curve depicting the thermal transformation of La(OH)$_2$Cl indicates two steps of mass loss (Fig. 7). As shown in Fig. 8a, the XRD pattern of the annealed product at approximately 360 °C is lanthanum oxychloride (LaOCl). The experimental mass loss of nearly 8.68 mass% (La(OH)$_2$Cl to LaOCl) corresponds well with the theoretical values (8.64 mass%). Fig. 8b shows the SEM image of the annealed product. The morphology of LaOCl particles synthesized according to the above steps is a thick platy aggregate. From the TG curve, we also can get that the mass declines slowly from about 480 °C. But there is no obvious peak in the DSC curve between 480 °C and 1500 °C. Lanthanum oxide is expected to form at approximately 480 °C. Increasing the annealing temperature to 1500 °C results in a material with all reflections corresponding to the La$_2$O$_3$ phase (Fig. 8c). From these results, we can infer that the phase transformation of LaOCl to La$_2$O$_3$ is slow. Similar result can be found from Zhu's article.[12] The only difference is that pure La$_2$O$_3$ can be obtained when the annealing temperature is increased to 1050 °C. Fig. 8d shows that the morphology of La$_2$O$_3$ is a short rod aggregate.
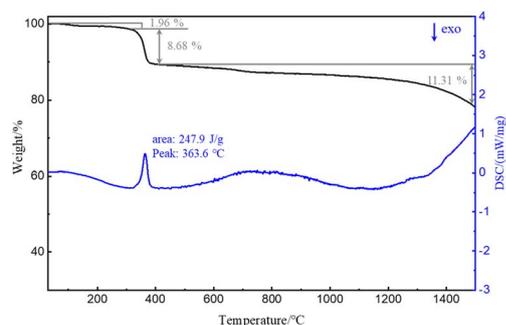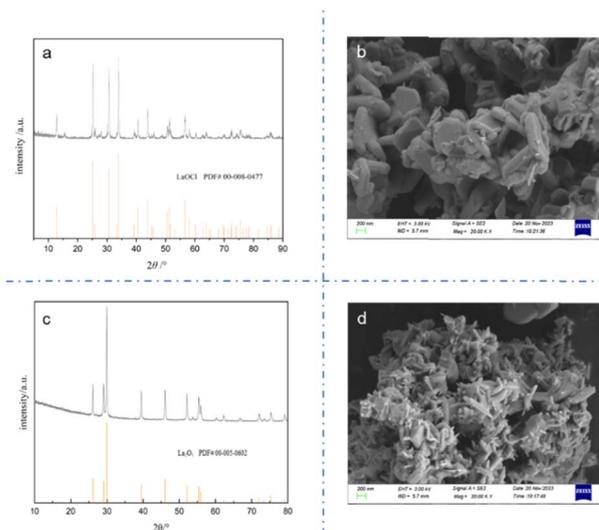

Fig. 7 TG-DSC result of sample 5.

Fig. 8 (a) XRD patterns of the annealed product at approximately 360 °C. (b) SEM image of the annealed product at approximately 360 °C. (c) XRD patterns of the annealed product at 1500 °C. (d) SEM image of the annealed product at 1500 °C.

4. Conclusions

To summarize, we explored a reactive crystallization method to synthesize La(OH)$_2$Cl. This method offers the advantages of low-temperature, high yield and short cycle length, making it potentially suitable for industrial applications and representing a novel approach for the low-carbon development of the rare earth metallurgical process. Additionally, we investigated the influence of these main parameters on the product's phase and the importance of controlling them in conjunction to synthesize La(OH)$_2$Cl. The as-synthesized products were characterized using XRD, FTIR, SEM, and TEM techniques. These results showed that the optimal conditions were as follows: the concentration of NH$_4$Cl in the base solution was 4 mol L^{-1} and the reaction system was 80 °C. At the same time, the molar ratio of NH$_4$OH/La^{3+} dropped per minute should be controlled to be 3 : 1. Then, the thermal dehydration of La(OH)$_2$Cl was investigated using the DSC/TG studies. It showed that LaOCl could be obtained at about 360 °C. The phase transformation of LaOCl to La$_2$O$_3$ shows slow progress and it starts at about 500 °C. From the SEM images of the annealed products, La(OH)$_2$Cl synthesized by this method offers the possibility of becoming a precursor in the preparation of special morphology LaOCl and La$_2$O$_3$.

Data availability

The data that support the findings of this study are available from the corresponding authors (Jincheng Guo and Xihong Hao), upon reasonable request.

Conflicts of interest

There are no conflicts to declare.

Acknowledgements

References

1 R. J. Liu, Z. H. Zhao, X. Y. Sang, Z. Z. Zhang, D. Wei, G. G. Zhang, W. B. Zhang and Y. Gao, Study on Preparation of Lanthanum Carbonate with Mixed Precipitation Agent of Ammonium Bicarbonate and Ammonia, *Rare Met. Cem. Carbides*, 2017, **45**, 51.

2 J. C. Guo, H. Tian, X. Y. Wang, X. J. Zhang, Y. H. Zhang and L. X. Yu, Preparation of Lanthanum Carbonate with Mixed Precipitation Agent and Its Precipitation Crystallization Process, *J. Chin. Soc. Rare Earths*, 2023, **41**, 1126.

3 J. K. Zhang, S. L. Zheng, P. Li, Y. N. Yang, X. D. Guan, J. Y. Zhou and D. Y. Chen, Preparation of High Quality Lanthanum Carbonate and Lanthanum Oxide by Composite Precipitant, *J. Chin. Soc. Rare Earths*, 2022, **40**, 624.

4 B. Chris, A. Max, N. Karsten, J. N. Lars, F. Manfred, L. Stefan, S.-R. Baltazar, D.-R. Amandine, S. Seton, W. Henri, S. Oliver and R. Shahrzad, A review of technology and policy deep decarbonization pathway options for making energy-intensive industry production consistent with the Paris agreement, *J. Cleaner Prod.*, 2018, **187**, 960.

5 M. A. Quader, S. Ahmed, S. Z. Dawal and Y. Nukman, Present needs, recent progress and future trends of energy-efficient ultra-low carbon dioxide (CO₂) steelmaking (ULCOS) program, *Renewable Sustainable Energy Rev.*, 2016, **55**, 537.

6 T. T. Xu, X. D. Zheng, B. Ji, Z. H. Xu, S. F. Bao, X. Zhang, G. M. Li, J. F. Mei and Z. Y. Li, Green recovery of rare earth elements under sustainability and low carbon: a review of current challenges and opportunities, *Sep. Purif. Technol.*, 2024, **330**, 125501.

7 S.-S. Lee, C.-H. Joh and S.-H. Byeon, Highly enhanced blue-emission of LnOCl:Tm prepared by dehydration of Ln(OH)₂Cl:Tm (Ln = La and Gd), *Mater. Sci. Eng., B*, 2008, **151**, 163.

8 F. L. Carter and S. Levinson, The Hydrothermal Preparation, Single-Crystal Lattice Parameters, Decomposition Data for Some Lanthanide Dihydroxy Chlorides the Related Hydroxy Chloride, Yb₃O(OH)₅Cl₂, *Inorg. Chem.*, 1969, **8**, 2788.

9 R. F. Klevtsova and L. A. Glinskaya, The Crystal Structure of Pr(OH)₂Cl, Sm(OH)₂Cl, and Gd(OH)₂Cl, *J. Struct. Chem.*, 1969, **10**, 408.

10 S. G. Podkolzin, E. E. Stangland, M. E. Jones, E. Peringer and J. A. Lercher, Methyl Chloride Production from Methane over Lanthanum-Based Catalysts, *J. Am. Chem. Soc.*, 2007, **129**, 2569.

11 A. W. A. M. van der Heijden, V. Bellière, L. E. Alonso, M. Daturi, O. V. Manoilova and B. M. Weckhuysen, Destructive Adsorption of CCl₄ over Lanthanum-Based Solids: Linking Activity to Acid-Base Properties, *J. Phys. Chem. B*, 2005, **109**, 23993.

12 X. R. Zhu, L. J. Hope-Weeks, D. Ramirez, R. Baghi, V. R. Charles and Y. J. He, Controllable decomposition of lanthanum oxychloride through different annealing conditions, *J. Alloys Compd.*, 2019, **800**, 29.

13 Z. W. Shi, X. Zhang, Y. H. Zhao, J. Y. Wang and G. C. Zhu, Kinetics on Chlorination Process of La₂O₃ and CeO₂ by Ammonium Chloride, *Chin. J. Process Eng.*, 2005, **5**, 23.

14 C. Jouve, J. Marrot and D. Riou, β-Sm(OH)₂Cl: a new lamellar variety, *Acta Crystallogr.*, 2002, **58**, 14.

15 S. V. Mahajan, J. Hart, J. Hood, A. Everheart, M. L. Redigolo, D. S. Koktysh, E. A. Payzant and J. H. Dickerson, Synthesis of RE(OH)₂Cl and REOCl (RE = Eu, Tb) nanostructures, *J. Rare Earths*, 2008, **26**, 131.

16 H. Kim, M. Kim and S. H. Byeon, Ce⁴⁺/Ce³⁺ redox-controlled luminescence "off/on" switching of highly oriented Ce(OH)₂Cl and Tb-doped Ce(OH)₂Cl, *J. Mater. Chem. C*, 2017, **5**, 444.

17 N. Soto-Donoso, L. Favier, S. F. Villalobos, V. Paredes-García, T. Bataille, J. F. Marco, R. M. Hlihor, E. L. Fur and D. Venegas-Yazigi, Lanthanum hydroxychloride/anatase composite and its application for effective UV-light driven oxidation of the emergent water contaminant cetirizine, *Chem. Eng. Res. Des.*, 2003, **196**, 685.

18 A. J. A. Dunn, J. W. Annis, J. M. Fisher, D. Thompsett and I. R. Walton, Ce(OH)₂Cl and lanthanide-substituted variants as precursors to redox-active CeO₂ materials, *Dalton Trans.*, 2020, **49**, 14871.

19 M. Fellner, A. Soppelsa and A. Lauria, Heat-Induced Transformation of Luminescent, Size Tuneable, Anisotropic Eu:Lu(OH)₂Cl Microparticles to Micro-Structurally Controlled Eu:Lu₂O₃ Microplatelets, *Crystals*, 2021, **11**, 992.

20 M. Mousavi-Kamazani, S. Alizadeh, F. Ansari and M. Salavati-Niasari, A controllable hydrothermal method to prepare La(OH)₃ nanorods using new precursors, *J. Rare Earths*, 2015, **33**, 425.

21 N. Imanak, T. Masui and Y. Kato, Preparation of the cubic-type La₂O₃ phase by thermal decomposition of LaI₃, *J. Solid State Chem.*, 2005, **178**, 395.

22 J. Feng, X. H. Li, M. Z. Wang, X. L. Zheng, J. T. Bai, L. Wang and Y. Peng, One-pot, template-free synthesis of hydrophobic single-crystalline La(OH)₃ nanowires with tunable size and their d⁰ ferromagnetic properties, *RSC Adv.*, 2015, **5**, 16093.

23 Y. Chen, Q. Qian, X. Liu, L. Xiao and Q. Chen, LaOCl nanofibers derived from electrospun PVA/lanthanum chloride composite fibers, *Mater. Lett.*, 2010, **64**, 6.

24 S.-S. Lee, H.-I. Park, C.-H. Joh and S.-H. Byeon, Morphology-dependent photoluminescence property of red-emitting LnOCl:Eu (Ln = La and Gd), *J. Solid State Chem.*, 2007, **180**, 3529.